Hydrodeoxygenation of m-cresol as a depolymerized lignin probe molecule: Synergistic effect of NiCo supported alloys

Vinicius Ottonio O. Gonçalves, Walter Henrique S.M. Talon, Vinicius Kartnaller, Fabricio Venancio, João Cajaiba, Thierry Cabioc'h, Jean-Marc Clacens, Frédéric Richard

Hydrodeoxygenation of m-cresol as a depolymerized lignin probe molecule: synergistic effect of NiCo supported alloys.

Vinicius Ottonio O. Gonçalves[1,2,3], Walter Henrique S.M. Talon[2], Vinicius Kartnaller[2], Fabricio Venancio[2], João Cajaiba[2], Thierry Cabioc'h[3], Jean-Marc Clacens[4], Frédéric Richard[4,*]

[1] Universidade Federal do Rio de Janeiro, Instituto de Química, Departamento de Físico-Química, Av. Athos da Silveira Ramos, nº 149, CEP 21949-900, Rio de Janeiro, RJ, Brazil

[2] Núcleo de Desenvolvimento de Processos e Análises Químicas em Tempo Real - NQTR, Universidade Federal do Rio de Janeiro, Instituto de Química, Rua Hélio de Almeida 40, Cidade Universitária, CEP 21941-614, Rio de Janeiro, Rio de Janeiro, RJ, Brazil

[3] Institut Pprime, UPR 3346 CNRS, Université de Poitiers – ISAE-ENSMA, BP 30179, 86962 Futuroscope-Chasseneuil Cedex, France.

[4] Institut de Chimie des Milieux et Matériaux de Poitiers, UMR 7285 Université de Poitiers - CNRS, 4, rue Michel Brunet, BP633, 86022 Poitiers Cedex, France.

Corresponding author: frederic.richard@univ-poitiers.fr

Keywords: m-cresol; hydrodeoxygenation; NiCo Alloy; bimetallic

Abstract

Three bimetallic Ni-Co (Ni:Co ratio 1:3, 1:1 and 3:1) and two monometallic (Ni and Co) nanoparticles supported on Al_2O_3 were synthesized by incipient wet impregnation and characterized by various technics (N_2-physisorption, XRD, H_2-TPR, CO-chemisorption and elemental analysis). It was demonstrated by XRD that NiCo alloys nanoparticles were present on bimetallic solids. The catalytic properties of all catalysts were determined for the hydrodeoxygenation of m-cresol at 340 °C under 4 MPa of total pressure. It was demonstrated that NiCo alloy developed better deoxygenation catalytic properties than pure Ni metallic phase, these properties being evaluated both by the total reaction rate (k_{TOT}) and the selectivity into deoxygenation products. Indeed, bimetallic NiCo(3:1)/Al_2O_3 was 1.2 times more active than Ni/Al_2O_3 and 8.8 times than Co/Al_2O_3, deoxygenated products being favored on bimetallic catalysts compared to Ni one. In addition, the k_{TOT} values seems to be related to the amount of CO uptakes, indicating that active sites in HDO were of similar nature than those allowing the adsorption of CO, and could be oxygen vacancies which were promoted in bimetallic NiCo particles.

1. Introduction

Bio-oil from biomass pyrolysis is becoming attractive to produce non-petroleum based and value-added biofuels and chemicals [1–4]. It contains a range of various organic compounds such as phenols, acids, aldehydes, and ketones, depending on the pyrolysis conditions and the biomass source [5]. The as-produced bio-oil remains low valuable as a product since it requires a decrease of its oxygen content to be more profitable. Hydrodeoxygenation (HDO) catalytic process can be used for oxygen removal. In recent years, much efforts were done in order to design a cost-effective catalyst for a HDO efficient process [6–12].

In this context, the catalyst must provide an acceptable combination of the followed features: stability, sustainability, deoxygenation rate, and selectivity toward more valuable products. Firstly, commercial sulfided solids such as Mo-based sulfides appeared as efficient catalysts for HDO and were extensively studied due to their interesting features as catalysts [13]. However, in the research of more sustainable processes, sulfided catalysts become limited since their use requires an S-containing agent (e.g. H_2S or dimethyl disulfide) to be present in the feed to maintain the catalyst activity. Unfortunately, their presence can lead to a possible sulfur contamination of the upgraded bio-oil liquids [14]. Noble metal catalysts (e.g. containing Pt or Pd) also exhibit attractive catalytic properties such as high activity and stability without the use of unsustainable materials such as sulfur [15,16]. However, these solids have high cost, meaning that the final product would be too expensive to compete with their petro-based similar compounds.

In the perspective to use an efficient catalyst with an affordable cost, the catalytic properties of nickel-based catalyst materials were recently investigated for the deoxygenation of triglycerides [17]. It is often proposed that active metallic phase containing at least two

components exhibits better catalytic characteristics compared to monometallic [18]. It is often reported that the catalytic properties of Ni-Co alloys were more interesting than the monometallics for various reactions such as partial oxidation of CH_4 [19]. CO hydrogenation [20,21], steam reforming of various substrates (CH_4 [22–27], biomass tar [28], ethanol [19,29,30], acetic acid [22] or glycerin [31]). The promoting effects due to the presence of alloys are mostly attributed to a better dispersion of metallic phase [23,32], to electronic effects [20], or to the enhancement of their reducibility properties [28,29]. Such behavior was also observed for Ni based catalysts. The association of Ni to different metals such as Cu [33,34], Re [35,36], Pd [37], Pt [37,38], Fe [39–43] or Co [44–50] leads to beneficial changes in their HDO catalytic properties. The presence of Ni-Cu alloys in the corresponding bimetallic catalysts favored the deoxygenation rate of anisole into methylcyclohexane under high pressure (6 MPa) at 280 °C. This promotion was linked to an increase in the nickel content [33]. In the same way, Yang et al. [36] showed a beneficial effect of the presence of Re in Ni-Re catalysts for the HDO of m-cresol under atmospheric pressure at 300°C. This effect was related to an increase of the Ni dispersion due to the presence of Re allowing the formation of active Ni-Re alloys. In the same way, Han et al. [43] reported that the bimetallic Ni-Fe catalyst was more active than the monometallic Ni one in HDO of phenol due to the presence of Ni-Fe alloy. In this last case, the bimetallic catalyst presented the highest HDO activity which was assigned to an increase of the adsorption strength of cyclohexanol on Ni-Fe alloy particles. This alcohol is an oxygenated product produced during the HDO of phenol, which can be transformed into cyclohexane by hydrogenolysis. It was also reported in literature that the presence of iron can modify the product distribution observed on Ni-based catalysts during HDO of m-cresol (300 °C, atmospheric pressure) [40]. Indeed, methylcyclohexanone was the main product over Ni/SiO_2 whereas toluene was predominant over $Ni\text{-}Fe/SiO_2$. According to the study, this change of selectivity in the presence of iron

could suppress the hydrogenation of the phenol aromatic ring. The authors proposed that iron could cause a repulsion with the π electron system of the phenol aromatic ring thereby inhibiting the hydrogenating properties of Ni-Fe particles. Using an acidic support (HZSM5 zeolite), Huynh et al. [44] demonstrated a beneficial effect of Co when it was associated to Ni for the HDO of phenol (5 MPa, 250 °C). In another case, studying guaiacol as model molecule at 400 °C under atmospheric pressure, Tran et al. [48] observed that the presence of Co enhanced the HDO activity of Ni based catalysts by favoring the dispersion of nickel metal oxides. Nevertheless, in both cases, the promoting effect of Co was difficult to estimate due to the very high level of conversion of phenol (close to 98 %). Recently, Liu et al. [49] reported that bimetallic NiCo alloys supported on Al_2O_3 were efficient catalysts for the HDO of vanillin, methylcyclohexanol being selectively produced at 2 MPa and 200 °C. Interestingly, the Co/Ni atomic ratio of 2 allowed to obtain a very high HDO performance since the yield in methylcycloghexanol was close to 100%. Such promoting effect was explained by the presence of electron-rich Co^0 species in CoNi nanoparticles which favored the activation of oxygen-containing groups.

In the present work, the investigation of nickel and cobalt alloys supported on γ-Al_2O_3 for the hydrodeoxygenation of m-cresol as bio-oil model compound under high hydrogen pressure was studied for the first time. The interest of studying such materials is based on the non-use of deleterious materials and on their potential effectiveness as catalysts for HDO. The relationship between the solids' properties and their performances as catalyst is discussed further herein.

2 Experimental

2.1 Catalyst preparation

Ni-Co catalysts were prepared by incipient wetness impregnation method of γ-alumina. Different molar ratios between cobalt and nickel were used in the synthesis using the correct amounts of $Ni(NO_3)_2.6H_2O$ and $Co(NO_3)_2.6H_2O$ as precursors (purchased from Sigma-Aldrich). In order to evaluate the bimetallic catalyst system, Ni/Al_2O_3 and Co/Al_2O_3 were also synthesized. The total metal loading (Co + Ni) was set to 10 wt.%. After impregnation, the catalyst was left for maturation during 5 days at 25 ºC. This aging time was already reported to ensure homogeneity between different elements in the case of co-impregnation procedure [51].

The impregnated solid was then calcinated at 500 ºC (1.5 ºC min^{-1}) for 5 h in a static oven. Further, the obtained catalysts were pelleted, crushed and sieved (250–315 µm).

2.2 Catalyst characterization

The Ni and Co contents of the catalysts were determined by atomic absorption using an AA200 Perkin Elmer equipment. Before analysis, the catalysts were solubilized in an acidic aqueous solution containing both hydrochloric and nitric acids.

N_2 adsorption−desorption isotherms were measured on a Micromeritics ASAP 2000 analyzer at -196 ºC. Prior to N_2 adsorption, the powder samples were degassed under secondary vacuum at 200 ºC overnight. The specific surface area was calculated using the Brunauer-Emmett-Teller (BET) method. The total pore volume was calculated from the adsorbed volume of nitrogen at P/P_0 equal to 0.99.

H_2-TPR measurements were performed for 100 mg of each catalyst in Autochem 2920. The solid was first pretreated under He flow (20 mL min^{-1}) at 200 ºC (10 ºC min^{-1}) for 30 min. Temperature was then adjusted to 50 ºC and the reduction measurements using TCD detector started under 10% H_2 in Ar (20 mL min^{-1}) until 1000 ºC (5 ºC min^{-1}) and kept in isotherm for 90 min.

X-ray diffraction (XRD) analysis were performed on a Bruker AXS D8 Advance diffractometer to determine the crystal structure of nanoparticles. The X-ray diffractometer was operated at 40 kV and 35 mA with a Co-Kα (λ = 1.7889 Å) X-ray source. Each analysis was performed for 2θ values from 20 to 100°, with steps of 0.05° and fixed acquisition time of 6s per step. Rietveld refinements of the diffractograms were performed using the Materials Analysis Using Diffraction (MAUD) software [52]. Prior to analysis, the Ni-Co solids were reduced in situ at 500 ºC (5 ºC min^{-1}) under 4 MPa of H_2 during 3 h by a flow of hydrogen (4.7 NL h^{-1}). After this procedure, samples were cooled down under hydrogen until room temperature and passivated under atmospheric pressure for 3 h using 5% O_2/He (80 mL min^{-1}).

CO chemisorption was determined by pulse method at 30 ºC. The catalyst was reduced in-situ at 500 ºC (3 h) at 4 MPa of H_2 as described above for X-ray analysis. The samples were transferred under argon atmosphere to an equipment for CO chemisorption measurements. First, the solid was pretreated with helium (30 mL min^{-1}) at 200 ºC for 30 minutes. Temperature was then set to 30 °C and CO pulses were injected until saturation. The measurements were detected by TCD.

The acidity of the support and catalysts was determined by NH_3-TPD. Experiments were performed on a Micromeritics Autochem 2910 apparatus. All samples were pretreated with pure He at 200°C during 1 h. The temperature was then lowered to 100 °C. The solid

was saturated with anhydrous NH_3 (10 vol% in He). Thereafter, it was purged under He, then the temperature was raised to 600 °C (heating rate: 5 °C min^{-1}). The amount of NH_3 desorbed was quantified by TCD.

Carbon content was determined using an elementary analyzer (NA2100 Protein Thermoquest, CE instruments). The catalysts were exposed to 1020 ºC under oxygen atmosphere. The C content was quantified by the analysis of CO_2 provided by the combustion of the solid.

2.3 Catalytic experiments

Ni-Co catalysts were tested in a continuous fixed-bed reactor for the deoxygenation of m-cresol at 340 °C under 4 MPa of total pressure. Prior to the reaction, each catalyst was reduced in-situ at 500 ºC (5 ºC min^{-1}) under 4 MPa of pure hydrogen (4.7 L/h) for 3 h. Temperature was then set to the reaction temperature (340 ºC). The reactor was fed by a liquid model feed composed of m-cresol (4.65 wt.%) and n-heptane as an internal standard (2.52 wt.%), in dodecane (solvent). The used molar ratio of hydrogen to m-cresol was 486 NL/L and the H_2 partial pressure was 3.24 MPa. All chemicals used in this study were purchased from Sigma-Aldrich, except for pure H_2 (Air Liquide).

During the reaction, the exit line of the reactor was refrigerated by a Minichiller-Huber at 10 ºC and the condensed samples were analyzed every hour using a Varian 430 chromatograph with a DB1 capillary column (length: 30 m, inside diameter: 0.320 mm, film thickness: 5 µm) and a FID detector.

The conversion and selectivity were calculated based on the following Eqs. (1) and (2), standard deviation of all values were estimated to 5%:

$$X_{CRE}(\%) = \frac{C^0_{CRE} - C_{CRE}}{C^0_{CRE}} \cdot 100 \quad (1)$$

$$S_i(\%) = \frac{C_i}{C^0_{CRE} - C_{CRE}} \cdot 100 \quad (2)$$

with C^0_{CRE} and C_{CRE} as the molar concentrations of m-cresol in the feed and in the collected liquid sample; C_i is the molar concentration of a given product.

Experiments were carried out during 25 h on stream. Different conversion levels were obtained using several space times (τ in g h mol^{-1}), changing the reactant flow (Eq. (3)).

$$\tau = \frac{W}{F_{CRE}} \quad (3)$$

where W is the weight of catalyst and F_{CRE} the molar flow of m-cresol.

The reactant and product concentration can be used to determine kinetic parameters of transformation of m-cresol. Assuming this reaction as 1st-order (Eq. (4)):

$$k_{TOT} = \frac{1}{\tau}\ln\left(1 - X_{CRE}\right) \quad (4)$$

where k_{TOT} is the reaction rate constant (mmol g^{-1} h^{-1}).

The turnover frequency (TOF, in h^{-1}) was calculated by Eq. (5):

$$TOF = \frac{k_{TOT}}{M} \quad (5)$$

where M is the CO uptake (in mmol g^{-1}) obtained from chemisorption experiments.

3 Results and discussion

3.1 Catalyst characterization

Ni and Co contents in the prepared catalysts were very close to the nominal values as shown in Table 1. The N_2 adsorption and desorption isotherms for the support and the catalysts reduced in situ at 4 MPa and 340 ºC are presented in Fig. 1. All catalysts possessed a mesoporous structure very similar to their support presenting a type IV isotherm. The fresh catalysts in oxide form also presented the same kind of isotherm (not shown here). Table 1 summarizes the textural properties of the support, the as prepared and reduced catalysts. For supported materials, raw values were recalculated to remove the contribution of oxide phases weight on textural properties (values in brackets in Table 1) allowing to access information on stability of the support during the impregnation-reduction steps. It can be noted that the values of surface area and pore volume of all solids slightly decreased after introduction of oxide phases. This result might be attributed to two factors, the formation of Ni and Co oxides blocking the support pores and the formation of a solid structure in the form of spinel species [29]. The reduction process led to a slight decrease of both S_{BET} and pore volume (less than 3%), showing that the reduction step preserves the textural properties of the catalysts. However, the surface areas of both Co/Al_2O_3 and Ni/Al_2O_3 were similar, close to 195 $m^2\ g^{-1}$.

Fig. 2 shows the TPR profiles of Ni/Al_2O_3, Co/Al_2O_3 and $NiCo/Al_2O_3$ with different molar ratios. The H_2 uptakes obtained from TPR measurements as well as the theoretical value assuming fully reduction of the metals can be found in Table 2. From these values, Ni and Co species were completely reduced to metallic species. The order of H_2 consumption followed Co/Al_2O_3 > NiCo (1:3)/Al_2O_3 > NiCo (1:1)/Al_2O_3 > NiCo (3:1)/Al_2O_3 > Ni/Al_2O_3, which is the expected order since NiO has the lowest hydrogen consumption and the spinel Co_3O_4 the highest one. In the case of Co/Al_2O_3, the first reduction peak is attributed to the reduction of

Co_3O_4 into CoO (360 ºC) and the second one to the reduction of CoO to metallic Co (574 ºC) [53,54]. For Ni/Al_2O_3, a wide reduction peak is observed at 665 ºC for the reduction of NiO small crystallites into Ni(0). A small shoulder at 824 ºC is due to the reduction of spinel $NiAl_2O_4$ [29,55,56]. It can be seen that the addition of nickel seems to favor the reduction of Co_3O_4 into CoO. Indeed, the peak observed at 360 °C without Ni shifts to lower temperature in the presence of Ni, which appeared at 287 °C for $NiCo(3:1)/Al_2O_3$. For the three solids having both Ni and Co, the reduction peaks of NiO and CoO species appearing between 400 and 800 °C became much closer; a single peak at around 550 °C is noted for the sample with the Ni to Co ratio equal to 3:1. This result indicates the formation of a bimetallic alloy Ni-Co during the reduction process. Indeed, it was proposed that the reducibility of Ni and Co species was simultaneously improved in NiCo samples [32,49]. In addition, the reduction of spinel $NiAl_2O_4$ species occurs at much higher temperature with the increase of cobalt content as already reported [29]. In order to verify that all metallic phases were reduced under the reduction step carried out prior the catalytic test (500 ºC, 4 MPa), additional TPR experiments were carried out for each pre-treated sample. The reactor was open in a glovebox filled with Argon and the reduced catalysts were transferred under Ar atmosphere to perform TPR. Over all reduced samples, no consumption of hydrogen was detected indicating that all oxide phases were totally reduced at 500 °C under 4 MPa of hydrogen pressure.

Fig. 3 displays the XRD diffraction patterns of Ni, Co and CoNi catalysts after being reduced at 4 MPa of H_2 at 500 ºC. Rietveld refinement of the diffractograms were performed to determine the crystallite size of the different catalysts by using popar rules [57] for the grain shape and for the microstrain. Excellent refinement of all the diffractograms were obtained (factor of goodness varying between 1.4 and 1.9) as shown in Fig. 4 allowing a precise determination of the lattice parameters and of the crystallite size (the uncertainty for the crystallite size is typically ± 1 nm). No spinel species were observed in the X-ray patterns, the

reduction step used was hence able to reduce mono- and bimetallic particles. The XRD patterns of supported monometallic solids (Ni/Al_2O_3 and Co/Al_2O_3) exhibited the characteristic lines of Ni^0 (JCPDS 98-016-2279; 2θ = 52.2, 61.1 and 91.9 °) and Co^0 (JCPDS 98-062-2443; 2θ = 51.8, 60.6 and 91.1°). The other observed peaks were attributed to γ-Al_2O_3 (JCPDS 00-050-0741). In the presence of bimetallic Ni-Co phase, the peaks previously attributer to Ni or Co were located between the Ni and Co metal peaks and shifted to smaller angle gradually with increasing Co amount. Fig. 5 shows a linear relationship between the lattice parameter (calculated by Rietveld refinements) and the composition of metallic phase estimated by the Ni/(Ni+Co) atomic ratio. This result is in agreement with the Vegard's law [58] and confirms the presence of Ni-Co alloy in bimetallic samples. In addition, the size of metallic nanoparticles seems to increase with the introduction of cobalt, in agreement with results reported by Wang et al. [28].

As expected, the acidity of the support and catalysts, determined by NH_3-TPD, was close to 1.0 µmol g^{-1} (Table 2), irrespective the presence and the nature of the metallic phase.

The value of CO uptake for Ni/Al_2O_3 is about twice higher than the one of Co/Al_2O_3 (Table 2), in agreement with results obtained by Takanabe et al. [59]. Interestingly, the bimetallic solid with a Ni/Co molar ratio close to 3 ($NiCo(3:1)/Al_2O_3$), shows the highest CO uptake. This alloy composition seems to favour the amount of sites allowing to adsorb CO.

3.2 HDO of m-cresol

The HDO of m-cresol was carried out at 4 MPa and 340 ºC in order to evaluate the effect of alloying nickel and cobalt. For each catalyst, experiments were performed for 25 h on stream and space time was changed every 5 h in order to study the evolution of the reaction products with the conversion of m-cresol (Fig. 6). In a run with high value of space time using the bare support as catalyst, no conversion of the reactant was observed. All catalysts were

stable under our experimental conditions during the whole set of experiments, despite the presence of carbon over spent catalysts (Table 3).

Fig. 7 shows a linear correlation between -ln (1- X_{CRE}) and space time (τ) indicating that the reaction can be modeled by a first-order kinetic, as already reported for several types of catalysts [60,61]. Thus, the overall rate constant (k_{TOT}) determined for each catalyst (Table 4) showed that NiCo (3:1)/Al_2O_3 was the most active of the studied series. It was about 1.2 times more active than Ni/Al_2O_3 and 9 times more active than Co/Al_2O_3, showing a promoting effect of the presence of Ni-Co alloy for HDO of m-cresol. In addition, the Ni-Co alloys composition had an effect on their HDO catalytic properties: in our studied samples, the higher the nickel content is, the higher the HDO activity is. Indeed, the order of activity among Ni-Co catalysts followed NiCo (3:1)/Al_2O_3 > NiCo(1:1)/Al_2O_3 > NiCo(1:3)/Al_2O_3 . Interestingly, this trend was the same that the one obtained from the CO uptake (Table 2), as shown in Fig. 8. The evolution of both k_{TOT} and CO uptakes as a function of the active phase composition (determined by the Ni/(Ni + Co) ratio) followed the same trend. These results seem to indicate that the sites allowing to adsorb CO are the active sites in HDO of m-cresol. Consequently, such technique seems to be well appropriate to measure the amount of HDO active sites. Recently, it was proposed that the active sites present on CoNi nanoparticles could be surface electron-rich Co^0 species, which could interact with oxygen atom and favor the deoxygenation rate [49]. Due to the lower amount of active sites estimated by CO adsorption for Ni/Al_2O_3 (35 μmol g^{-1}) compared to NiCo(3:1)/Al_2O_3 (46 μmol g^{-1}), the TOF value of Ni/Al_2O_3 was about 1.1 times higher than the one of NiCo(3:1)/Al_2O_3 (Table 4), even if the total activity (estimated by k_{TOT}) of NiCo(3:1)/Al_2O_3 was 1.2 times higher than Ni/Al_2O_3. In addition, the TOF values reported in Table 4 indicates that the activity of Ni/Al_2O_3 was higher than the one of Co/Al_2O_3, in agreement with results obtained for HDO of phenol [44].

In order to highlight the promoting effect in HDO of the presence of Ni-Co alloy instead of neighboring Ni and Co metallic phases, the catalytic properties of NiCo(3:1)/Al_2O_3 were compared to the ones of a mechanical mixture composed by 75 wt.% of Ni/Al_2O_3 and 25 wt.% of Co/Al_2O_3. As highlighted in Fig. 7, the former was about 1.7 times more active than the latter, showing the advantage of the presence of Ni-Co alloys to favor the HDO catalytic properties of bimetallic Ni-Co solids, especially when NiCo(3:1) phase was formed. Under the same experimental conditions (340 °C, 3 MPa), the HDO of m-cresol was already reported over various supported catalytic systems, such as molybdenum sulfide [62], molybdenum oxide [63] and nickel phosphides [60,61,64]. Only CoMoS/Al_2O_3 was slightly more active than the NiCo(3:1)/Al_2O_3 (about 1.1 times more active). Nevertheless, the selectivity of this sulfide phase was different since toluene was the main product over CoMo/Al_2O_3.

In addition, except to Co/Al_2O_3, the particle size increases linearly with the amount of Co (Fig. 5). This trend was rather different that the one observed for the HDO activity, indicating that the particle size of the metallic nanoparticles (monometallic or alloy) was probably not a key parameter to explain their catalytic properties, as previously suggested [44,59].

Fig. 9 displays the influence of time on stream on both conversion and selectivity for the transformation of m-cresol (τ = 5 g h mol^{-1}) over NiCo (3:1)/Al_2O_3 under 4 MPa and 340 °C. Under these experimental conditions, m-cresol was mainly deoxygenated into methylcyclohexane (~ 56 mol%) and methylcyclohexenes (~ 33 mol%). Toluene was also detected but in low quantities (less than 2 mol%). An oxygenated compound, methylcyclohexanone, was also observed in the reactional mixture; its amount being close to 10 mol%. As indicated in Table 4, the presence of Co favored the total deoxygenation of m-cresol since the HDO values were higher than 90 mol% for the three bimetallic catalysts and

for Co/Al_2O_3, whereas deoxygenation selectivity was lower for Ni/Al_2O_3 (equal to 84 mol.%) showing that the presence of Co^0 species favored the activation of m-cresol. Such behavior was already reported by Liu et al. [49] and attributed to the presence of surface oxygen-vacancy which decorated bimetallic CoNi nanoparticles. In addition, the proportion of methylcyclohexane was the highest on $NiCo(3:1)/Al_2O_3$ (56 mol%) and the lowest on Co/Al_2O_3 (41 mol.%). Our results are in accordance with results reported by Huynh et al. [44] using phenol as probe molecule, cyclohexane being the main product (250°C, 5 MPa). However, over Co/Al_2O_3, methylcyclohexenes become the major products, showing the lower hydrogenating properties of Co compared to Ni. In the same way, Co seems more selective into toluene than Ni. According to Table 4, the degree of deoxygenation (HDO %) is favored by increasing the Co content. Zhou et al. [46] observed that the selectivity into cyclohexanol in the HDO of guaiacol was improved using nickel catalyst promoted by cobalt; this catalyst being supported on carbon nanotubes; meanwhile pure nickel mostly produced catechol, a product obtained without oxygen removal. Similarly, for the hydrodeoxygenation of guaiacol under 1 MPa and at 300 ºC, Mochizuki et al. [65] showed that the degree of deoxygenation over Co/SiO_2 was higher, leading mainly to aromatic and naphthenic compounds, than Ni/SiO_2, which gave cyclohexanol as main product.

Fig. 10 shows the behavior of the selectivity from the transformation of m-cresol as function of space times. At low conversion levels (low contact time values) alkene isomers (methylcyclohexenes) were preferentially formed, their selectivity decreased by increasing the conversion of the phenolic reactant. Regarding the evolution of selectivity with m-cresol conversion, 3-methylcyclohexanone followed the same trend than methylcyclohexenes. At higher space times, methylcyclohexane selectivity increases until it becomes the major product. The selectivity into toluene was not modified in the range of contact time studied for each catalyst.

From previous results over several active phases (CoMoS, Ni, Ni_2P, MoO_x) [60–64], it can be admitted that the transformation of phenolic compounds proceeds mainly via two parallel routes. Products of m-cresol ring hydrogenation are favored over NiCo catalysts, and are formed by the so-called HYDdrogenation route, which proceeds from the adsorption of m-cresol leading first to 3-methylcyclohexanone. The hydrogenation of its C=O bond leads to 3-methylcyclohexanol. This alcohol was never observed in these experimental conditions owing to its high reactivity through dehydration reaction. Such results were also described in the literature when acid supports like Al_2O_3 were used for HDO of alkylphenols [63,66,67]. The acidity of the catalytic support alone, determined by NH_3-TPD, was close to 1.04 μmol g^{-1}, which was practically unmodified in the presence of reduced Ni and/or Co nanoparticles (Table 2). Methylcylohexene isomers (MCHes) were hence produced from dehydration of 3-methylcyclohexanol, which may occur on alumina acid sites. Interestingly, 1-methylcyclohexene was always the main alkene isomer instead of the expected isomers, being about 63 mol% of all alkene isomers (Table 4). This value was close to the percentage calculated from thermodynamics (65 mol%), suggesting isomerization until thermodynamic equilibrium [68]. This observation was also reported for catalysts exhibiting acidic properties [62,63].

By the HYD route, methylcyclohexane is then obtained via the alkene hydrogenation. The other pathway leads to the direct scission of C-O bond forming toluene being called direct deoxygenation (DDO route). The proposed reaction pathways for the transformation of m-cresol is shown in Scheme 1.

The addition of nickel in the Co/Al_2O_3 strongly enhances the hydrogenating properties of the solid, which can be seen by the ratio of methylcyclohexane to methylcyclohexenes that increases with Ni content (Table 4). This result is expected since nickel is known for its ability to hydrogenate even hard refractory aromatics such as benzene [69]. From the aromatic

selectivity order, NiCo catalyst tends to break the C-O bond leading to toluene by increasing the Co content, even if it is in a small extent. Indeed, the synergistic effect between cobalt and nickel forming an alloy increases the metal dispersion and leads to a stronger catalytic site compared to the physical mixture.

4 Conclusion

In this work, the hydrodeoxygenation of m-cresol was carried out at 340 °C under 4 MPa over monometallic Ni and Co nanoparticles and various bimetallic Ni-Co systems, all metallic phases were supported on Al_2O_3. It was demonstrated that NiCo alloys were formed in bimetallic systems. The catalyst having a Ni/Co atomic ratio close to 3 (NiCo(3:1)/Al_2O_3) was the most active one. A synergistic effect between Ni and Co due to the presence of NiCo alloy was highlighted. Nickel enhanced the hydrogenating properties of the catalyst whereas the addition of cobalt favored the deoxygenation rate of m-cresol due to the presence of CoNi nanoparticles which favored the formation of oxygen vacancy acting as deoxygenation active site. All catalysts remained stable during experimental conditions despite carbon deposition probably due to the high hydrogen pressure.

5 References

[1] G.W. Huber, A. Corma, Synergies between Bio- and Oil Refineries for the Production of Fuels from Biomass, Angew. Chem. Int. Ed. 46 (2007) 7184–7201. https://doi.org/10.1002/anie.200604504.

[2] C. Li, X. Zhao, A. Wang, G.W. Huber, T. Zhang, Catalytic Transformation of Lignin for the Production of Chemicals and Fuels, Chem. Rev. (2015) 151019104555004. https://doi.org/10.1021/acs.chemrev.5b00155.

[3] T. Kan, V. Strezov, T.J. Evans, Lignocellulosic biomass pyrolysis: A review of product properties and effects of pyrolysis parameters, Renew. Sustain. Energy Rev. 57 (2016) 1126–1140. https://doi.org/10.1016/j.rser.2015.12.185.

[4] T.M.H. Dabros, M.Z. Stummann, M. Høj, P.A. Jensen, J.-D. Grunwaldt, J. Gabrielsen, P.M. Mortensen, A.D. Jensen, Transportation fuels from biomass fast pyrolysis, catalytic hydrodeoxygenation, and catalytic fast hydropyrolysis, Prog. Energy Combust. Sci. 68 (2018) 268–309. https://doi.org/10.1016/j.pecs.2018.05.002.

[5] G.W. Huber, S. Iborra, A. Corma, Synthesis of transportation fuels from biomass: chemistry, catalysts, and engineering, Chem. Rev. 106 (2006) 4044–4098.

[6] Q. Bu, H. Lei, A.H. Zacher, L. Wang, S. Ren, J. Liang, Y. Wei, Y. Liu, J. Tang, Q. Zhang, A review of catalytic hydrodeoxygenation of lignin-derived phenols from biomass pyrolysis, Bioresour. Technol. 124 (2012) 470–477.

[7] N. Arun, R.V. Sharma, A.K. Dalai, Green diesel synthesis by hydrodeoxygenation of bio-based feedstocks: Strategies for catalyst design and development, Renew. Sustain. Energy Rev. 48 (2015) 240–255.

[8] P.M. Mortensen, J.-D. Grunwaldt, P.A. Jensen, K. Knudsen, A.D. Jensen, A review of catalytic upgrading of bio-oil to engine fuels, Appl. Catal. Gen. 407 (2011) 1–19.

[9] X. Li, X. Luo, Y. Jin, J. Li, H. Zhang, A. Zhang, J. Xie, Heterogeneous sulfur-free hydrodeoxygenation catalysts for selectively upgrading the renewable bio-oils to second generation biofuels, Renew. Sustain. Energy Rev. 82 (2018) 3762–3797. https://doi.org/10.1016/j.rser.2017.10.091.

[10] W. Jin, L. Pastor-Pérez, D. Shen, A. Sepúlveda-Escribano, S. Gu, T. Ramirez Reina, Catalytic Upgrading of Biomass Model Compounds: Novel Approaches and Lessons Learnt from Traditional Hydrodeoxygenation – a Review, ChemCatChem. 11 (2019) 924–960. https://doi.org/10.1002/cctc.201801722.

[11] H. Baloch, S. Nizamuddin, M.T.H. Siddiqui, S. Riaz, A. Jatoi, D. Dumbre, N. Mubarak, M. Srinivasan, G. Griffin, Recent advances in production and upgrading of bio-oil from biomass: A critical overview, J. Environ. Chem. Eng. 6 (2018) 5101–5118. https://doi.org/10.1016/j.jece.2018.07.050.

[12] J.E. Peters, J.R. Carpenter, D.C. Dayton, Anisole and Guaiacol Hydrodeoxygenation Reaction Pathways over Selected Catalysts, Energy Fuels. 29 (2015) 909–916.

[13] E. Furimsky, Catalytic hydrodeoxygenation, Appl. Catal. Gen. 199 (2000) 147–190. https://doi.org/10.1016/S0926-860X(99)00555-4.

[14] E.-M. Ryymin, M.L. Honkela, T.-R. Viljava, A.O.I. Krause, Insight to sulfur species in the hydrodeoxygenation of aliphatic esters over sulfided NiMo/γ-Al 2 O 3 catalyst, Appl. Catal. Gen. 358 (2009) 42–48.

[15] C. Liu, Z. Shao, Z. Xiao, C.T. Williams, C. Liang, Hydrodeoxygenation of benzofuran over silica–alumina-supported Pt, Pd, and Pt–Pd catalysts, Energy Fuels. 26 (2012) 4205–4211.

[16] T. Nimmanwudipong, R.C. Runnebaum, D.E. Block, B.C. Gates, Catalytic conversion of guaiacol catalyzed by platinum supported on alumina: reaction network including hydrodeoxygenation reactions, Energy Fuels. 25 (2011) 3417–3427.

[17] C. Kordulis, K. Bourikas, M. Gousi, E. Kordouli, A. Lycourghiotis, Development of nickel based catalysts for the transformation of natural triglycerides and related compounds into green diesel: a critical review, Appl. Catal. B Environ. 181 (2016) 156–196.

[18] D.M. Alonso, S.G. Wettstein, J.A. Dumesic, Bimetallic catalysts for upgrading of biomass to fuels and chemicals, Chem. Soc. Rev. 41 (2012) 8075. https://doi.org/10.1039/c2cs35188a.

[19] A.C. Koh, L. Chen, W.K. Leong, B.F. Johnson, T. Khimyak, J. Lin, Hydrogen or synthesis gas production via the partial oxidation of methane over supported nickel–cobalt catalysts, Int. J. Hydrog. Energy. 32 (2007) 725–730.

[20] T. Ishihara, N. Horiuchi, T. Inoue, K. Eguchi, Y. Takita, H. Arai, Effect of alloying on CO hydrogenation activity over SiO2-supported Co-Ni alloy catalysts, J. Catal. 136 (1992) 232–241.

[21] T. Ishihara, K. Eguchi, H. Arai, Hydrogenation of carbon monoxide over SiO2-supported Fe-Co, Co-Ni and Ni-Fe bimetallic catalysts, Appl. Catal. 30 (1987) 225–238.

[22] X. Hu, G. Lu, Investigation of steam reforming of acetic acid to hydrogen over Ni–Co metal catalyst, J. Mol. Catal. Chem. 261 (2007) 43–48. https://doi.org/10.1016/j.molcata.2006.07.066.

[23] J. Zhang, H. Wang, A.K. Dalai, Development of stable bimetallic catalysts for carbon dioxide reforming of methane, J. Catal. 249 (2007) 300–310.

[24] J. Zhang, H. Wang, A.K. Dalai, Effects of metal content on activity and stability of Ni-Co bimetallic catalysts for CO 2 reforming of CH 4, Appl. Catal. Gen. 339 (2008) 121–129.

[25] S.M. Sajjadi, M. Haghighi, A.A. Eslami, F. Rahmani, Hydrogen production via CO2-reforming of methane over Cu and Co doped Ni/Al2O3 nanocatalyst: impregnation versus sol–gel method and effect of process conditions and promoter, J. Sol-Gel Sci. Technol. 67 (2013) 601–617. https://doi.org/10.1007/s10971-013-3120-8.

[26] D. San-José-Alonso, J. Juan-Juan, M. Illán-Gómez, M. Román-Martínez, Ni, Co and bimetallic Ni–Co catalysts for the dry reforming of methane, Appl. Catal. Gen. 371 (2009) 54–59.

[27] S. Das, M. Sengupta, A. Bag, M. Shah, A. Bordoloi, Facile synthesis of highly disperse Ni–Co nanoparticles over mesoporous silica for enhanced methane dry reforming, Nanoscale. 10 (2018) 6409. https://doi.org/10.1039/C7NR09625A.

[28] L. Wang, D. Li, M. Koike, H. Watanabe, Y. Xu, Y. Nakagawa, K. Tomishige, Catalytic performance and characterization of Ni–Co catalysts for the steam reforming of biomass tar to synthesis gas, Fuel. 112 (2013) 654–661.

[29] S. Andonova, C. De Ávila, K. Arishtirova, J. Bueno, S. Damyanova, Structure and redox properties of Co promoted Ni/Al 2 O 3 catalysts for oxidative steam reforming of ethanol, Appl. Catal. B Environ. 105 (2011) 346–360.

[30] L. Chen, C.K.S. Choong, Z. Zhong, L. Huang, Z. Wang, J. Lin, Support and alloy effects on activity and product selectivity for ethanol steam reforming over supported nickel cobalt catalysts, Int. J. Hydrog. Energy. 37 (2012) 16321–16332. https://doi.org/10.1016/j.ijhydene.2012.02.119.

[31] N. Luo, K. Ouyang, F. Cao, T. Xiao, Hydrogen generation from liquid reforming of glycerin over Ni–Co bimetallic catalyst, Biomass Bioenergy. 34 (2010) 489–495. https://doi.org/10.1016/j.biombioe.2009.12.013.

[32] J. Xu, W. Zhou, Z. Li, J. Wang, J. Ma, Biogas reforming for hydrogen production over nickel and cobalt bimetallic catalysts, Int. J. Hydrog. Energy. 34 (2009) 6646–6654.

[33] S.A. Khromova, A.A. Smirnov, O.A. Bulavchenko, A.A. Saraev, V.V. Kaichev, S.I. Reshetnikov, V.A. Yakovlev, Anisole hydrodeoxygenation over Ni–Cu bimetallic catalysts: The effect of Ni/Cu ratio on selectivity, Appl. Catal. Gen. 470 (2014) 261–270.

[34] A. Ardiyanti, S. Khromova, R. Venderbosch, V. Yakovlev, H. Heeres, Catalytic hydrotreatment of fast-pyrolysis oil using non-sulfided bimetallic Ni-Cu catalysts on a δ-Al 2 O 3 support, Appl. Catal. B Environ. 117 (2012) 105–117.

[35] B. Feng, H. Kobayashi, H. Ohta, A. Fukuoka, Aqueous-phase hydrodeoxygenation of 4-propylphenol as a lignin model to n-propylbenzene over Re-Ni/ZrO2 catalysts, J. Mol. Catal. Chem. 388–389 (2014) 41–46. https://doi.org/10.1016/j.molcata.2013.09.025.

[36] F. Yang, D. Liu, H. Wang, X. Liu, J. Han, Q. Ge, X. Zhu, Geometric and electronic effects of bimetallic Ni–Re catalysts for selective deoxygenation of m-cresol to toluene, J. Catal. 349 (2017) 84–97. https://doi.org/10.1016/j.jcat.2017.01.001.

[37] Q. Lai, C. Zhang, J.H. Holles, Hydrodeoxygenation of guaiacol over Ni@Pd and Ni@Pt bimetallic overlayer catalysts, Appl. Catal. Gen. 528 (2016) 1–13. https://doi.org/10.1016/j.apcata.2016.09.009.

[38] P.T. Do, A.J. Foster, J. Chen, R.F. Lobo, Bimetallic effects in the hydrodeoxygenation of meta-cresol on γ-Al 2 O 3 supported Pt–Ni and Pt–Co catalysts, Green Chem. 14 (2012) 1388–1397.

[39] S. Leng, X. Wang, X. He, L. Liu, Y. Liu, X. Zhong, G. Zhuang, J. Wang, NiFe/γ-Al 2 O 3: a universal catalyst for the hydrodeoxygenation of bio-oil and its model compounds, Catal. Commun. 41 (2013) 34–37.

[40] L. Nie, P.M. de Souza, F.B. Noronha, W. An, T. Sooknoi, D.E. Resasco, Selective conversion of m-cresol to toluene over bimetallic Ni–Fe catalysts, J. Mol. Catal. Chem. 388–389 (2014) 47–55. https://doi.org/10.1016/j.molcata.2013.09.029.

[41] H. Shafaghat, P.S. Rezaei, W.M.A.W. Daud, Catalytic hydrodeoxygenation of simulated phenolic bio-oil to cycloalkanes and aromatic hydrocarbons over bifunctional metal/acid catalysts of Ni/HBeta, Fe/HBeta and NiFe/HBeta, J. Ind. Eng. Chem. 35 (2016) 268–276.

[42] X. Liu, W. An, C.H. Turner, D.E. Resasco, Hydrodeoxygenation of m-cresol over bimetallic NiFe alloys: Kinetics and thermodynamics insight into reaction mechanism, J. Catal. 359 (2018) 272–286. https://doi.org/10.1016/j.jcat.2018.01.006.

[43] Q. Han, M.U. Rehman, J. Wang, A. Rykov, O.Y. Gutiérrez, Y. Zhao, S. Wang, X. Ma, J.A. Lercher, The synergistic effect between Ni sites and Ni-Fe alloy sites on hydrodeoxygenation of lignin-derived phenols, Appl. Catal. B Environ. 253 (2019) 348–358. https://doi.org/10.1016/j.apcatb.2019.04.065.

[44] T.M. Huynh, U. Armbruster, M.-M. Pohl, M. Schneider, J. Radnik, D.-L. Hoang, B.M.Q. Phan, D.A. Nguyen, A. Martin, Hydrodeoxygenation of Phenol as a Model Compound for Bio-oil on Non-noble Bimetallic Nickel-based Catalysts, ChemCatChem. 6 (2014) 1940–1951. https://doi.org/10.1002/cctc.201402011.

[45] T.M. Huynh, U. Armbruster, L.H. Nguyen, D.A. Nguyen, A. Martin, Hydrodeoxygenation of Bio-Oil on Bimetallic Catalysts: From Model Compound to Real Feed, J. Sustain. Bioenergy Syst. 5 (2015) 151.

[46] M. Zhou, Y. Wang, Y. Wang, G. Xiao, Catalytic conversion of guaiacol to alcohols for bio-oil upgrading, J. Energy Chem. 24 (2015) 425–431.

[47] M. Zhou, J. Ye, P. Liu, J. Xu, J. Jiang, Water-Assisted Selective Hydrodeoxygenation of Guaiacol to Cyclohexanol over Supported Ni and Co Bimetallic Catalysts, ACS Sustain. Chem. Eng. 5 (2017) 8824–8835. https://doi.org/10.1021/acssuschemeng.7b01615.

[48] N.T. Tran, Y. Uemura, S. Chowdhury, A. Ramli, Vapor-phase hydrodeoxygenation of guaiacol on Al-MCM-41 supported Ni and Co catalysts, Appl. Catal. Gen. 512 (2016) 93–100.

[49] M. Liu, J. Zhang, L. Zheng, G. Fan, L. Yang, F. Li, Significant Promotion of Surface Oxygen Vacancies on Bimetallic CoNi Nanocatalysts for Hydrodeoxygenation of Biomass-derived Vanillin to Produce Methylcyclohexanol, ACS Sustain. Chem. Eng. 8 (2020) 6075–6089. https://doi.org/10.1021/acssuschemeng.0c01015.

[50] T.K. Hari, Z. Yaakob, Production of diesel fuel by the hydrotreatment of jatropha oil derived fatty acid methyl esters over γ-Al2O3 and SiO2 supported NiCo bimetallic catalysts, React. Kinet. Mech. Catal. 116 (2015) 131–145.

[51] A. Ungureanu, B. Dragoi, A. Chirieac, S. Royer, D. Duprez, E. Dumitriu, Synthesis of highly thermostable copper-nickel nanoparticles confined in the channels of ordered mesoporous SBA-15 silica, J. Mater. Chem. 21 (2011) 12529–12541. https://doi.org/10.1039/C1JM10971E.

[52] L. Lutterotti, S. Matthies, H. Wenk, MAUD: a friendly Java program for material analysis using diffraction, IUCr Newsl. CPD. 21 (1999).

[53] Y. Ji, Z. Zhao, A. Duan, G. Jiang, J. Liu, Comparative study on the formation and reduction of bulk and Al2O3-supported cobalt oxides by H2-TPR technique, J. Phys. Chem. C. 113 (2009) 7186–7199.

[54] G. Jacobs, T.K. Das, Y. Zhang, J. Li, G. Racoillet, B.H. Davis, Fischer–Tropsch synthesis: support, loading, and promoter effects on the reducibility of cobalt catalysts, Appl. Catal. Gen. 233 (2002) 263–281.

[55] L. Zhang, X. Wang, B. Tan, U.S. Ozkan, Effect of preparation method on structural characteristics and propane steam reforming performance of Ni–Al 2 O 3 catalysts, J. Mol. Catal. Chem. 297 (2009) 26–34.

[56] S. Zhang, L. Li, B. Xue, J. Chen, N. Guan, F. Zhang, Selective catalytic reduction of nitric oxide with propane over Ni-Al 2 O 3: effect of Ni loading, React. Kinet. Catal. Lett. 89 (2006) 81–87.

[57] N.C. Popa, The (hkl) Dependence of Diffraction-Line Broadening Caused by Strain and Size for all Laue Groups in Rietveld Refinement, J. Appl. Crystallogr. 31 (1998) 176–180. https://doi.org/10.1107/S0021889897009795.

[58] B.D. Cullity, Elements of x-ray diffraction, Addison-Wesley Publishing Company, Inc., Reading, MA, 1978.

[59] K. Takanabe, K. Nagaoka, K. Nariai, K. Aika, Titania-supported cobalt and nickel bimetallic catalysts for carbon dioxide reforming of methane, J. Catal. 232 (2005) 268–275.

[60] V.O.O. Gonçalves, P.M. de Souza, T. Cabioc'h, V.T. da Silva, F.B. Noronha, F. Richard, Hydrodeoxygenation of m-cresol over nickel and nickel phosphide based catalysts. Influence of the nature of the active phase and the support, Appl. Catal. B Environ. 219 (2017) 619–628. https://doi.org/10.1016/j.apcatb.2017.07.042.

[61] V.O.O. Gonçalves, P.M. de Souza, V.T. da Silva, F.B. Noronha, F. Richard, Kinetics of the hydrodeoxygenation of cresol isomers over Ni2P/SiO2: Proposals of nature of deoxygenation active sites based on an experimental study, Appl. Catal. B Environ. 205 (2017) 357–367. https://doi.org/10.1016/j.apcatb.2016.12.051.

[62] V.O.O. Gonçalves, S. Brunet, F. Richard, Hydrodeoxygenation of Cresols Over Mo/Al2O3 and CoMo/Al2O3 Sulfided Catalysts, Catal. Lett. 146 (2016) 1562–1573. https://doi.org/10.1007/s10562-016-1787-5.

[63] V.O.O. Gonçalves, C. Ciotonea, S. Arrii-Clacens, N. Guignard, C. Roudaut, J. Rousseau, J.-M. Clacens, S. Royer, F. Richard, Effect of the support on the hydrodeoxygenation of m-cresol over molybdenum oxide based catalysts, Appl. Catal. B Environ. 214 (2017) 57–66. https://doi.org/10.1016/j.apcatb.2017.05.003.

[64] V.O.O. Gonçalves, P.M. de Souza, T. Cabioc'h, V.T. da Silva, F.B. Noronha, F. Richard, Effect of P/Ni ratio on the performance of nickel phosphide phases supported on zirconia for the hydrodeoxygenation of m-cresol, Catal. Commun. 119 (2019) 33–38. https://doi.org/10.1016/j.catcom.2018.09.015.

[65] T. Mochizuki, S.-Y. Chen, M. Toba, Y. Yoshimura, Deoxygenation of guaiacol and woody tar over reduced catalysts, Appl. Catal. B Environ. 146 (2014) 237–243.

[66] Y. Romero, F. Richard, S. Brunet, Hydrodeoxygenation of 2-ethylphenol as a model compound of bio-crude over sulfided Mo-based catalysts: Promoting effect and reaction mechanism, Appl. Catal. B Environ. 98 (2010) 213–223. https://doi.org/10.1016/j.apcatb.2010.05.031.

[67] C. Bouvier, Y. Romero, F. Richard, S. Brunet, Effect of H2S and CO on the transformation of 2-ethylphenol as a model compound of bio-crude over sulfided Mo-based catalysts: propositions of promoted active sites for deoxygenation pathways based on an experimental study, Green Chem. 13 (2011) 2441–2451. https://doi.org/10.1039/C1GC15181A.

[68] M. Peereboom, B. Van de Graaf, J.M.A. Baas, Experimental and calculated thermodynamic data for the isomeric methylcyclohexenes and methylenecyclohexane, Recl. Trav. Chim. Pays-Bas. 101 (1982) 336–338.

[69] T. Mokrane, A.-G. Boudjahem, M. Bettahar, Benzene hydrogenation over alumina-supported nickel nanoparticles prepared by polyol method, RSC Adv. 6 (2016) 59858–59864. https://doi.org/10.1039/C6RA08527J.

Acknowledgments

This research was founded by the Conselho Nacional de Desenvolvimento Científico e Tecnológico (CNPq), the Institute of Material and Environment Chemistry of Poitiers (IC2MP) and the University of Poitiers. Vinicius O.O. Gonçalves is grateful to the Brazilian program Science without Borders and to Université de Poitiers for the Invited Professor Grant. This research was supported by the CAPES-COFECUB program Ph-S_Sv 912/18. Walter Henrique S.M. Talon thanks the Scientific Initiation Program from Fundação de Amparo à Pesquisa do Estado do Rio de Janeiro (FAPERJ). Jean-Marc Clacens and Frédéric Richard acknowledge financial support from the European Union (ERDF) and "Région Nouvelle Aquitaine".

Figure Captions

Fig. 1. N_2 adsorption and desorption isotherms of the bare support and the reduced catalysts at 4 MPa and 340 ºC for 3h. (●) Adsorption (○) Desorption.

Fig. 2. H_2-TPR profiles of samples with different nickel and cobalt contents. Reduction conditions: 30 ml min^{-1} 10% of H_2 in Ar and heating rate 5 °C min^{-1}.

Fig. 3. XRD patterns of reduced samples at 500 ºC under 4 MPa of H_2. Al_2O_3: (◊, JCPDS: 00-050-0741); Ni^0: (▲, JCPDS: 98-016-2279); Co^0: (□: JCPDS: 98-062-2443), Ni-Co solid solution alloy (■).

Fig. 4: XRD diagram of Co/Al_2O_3 (a) and $NiCo(3:1)/Al_2O_3$ (b) samples (experimental data (black dots), refined data (red solid line)). Difference between the experimental data and the Rietveld refinement is given at the bottom of the figures.

Fig. 5: Influence of the Ni/(Ni + Co) ratio on the lattice parameter (in Å, ■) and the particle size (in nm, ▲) determined from XRD of reduced Ni-Co supported catalysts.

Fig. 6. Conversion as function of time on stream for the HDO of m-cresol during 25 h on stream (τ in g h mol^{-1}).

Fig. 7. Plots of -ln (1- X_{CRE}) as function of τ for HDO of m-cresol at 4 MPa and 340 ºC. Ni/Al_2O_3 (■); $NiCo(3:1)/Al_2O_3$ (▲); $NiCo(1:1)/Al_2O_3$ (×); $NiCo(1:3)/Al_2O_3$ (◆); Co/Al_2O_3 (●).

Fig. 8. Influence of the Ni/(Ni+Co) ratio of Al_2O_3 supported catalysts on the k_{TOT} values (■, left axis) obtained for HDO of m-cresol and the CO uptakes (▲, right axis). Mechanical

mixture composed by Ni/ Al_2O_3 (75 wt.%) and Co/Al_2O_3 (25 wt.%): k_{TOT} (□) and CO uptake (△).

Fig. 9. Conversion and selectivity as function of time on stream for NiCo (3:1)/Al_2O_3 at τ = 5 g h mol^{-1} at 4 MPa and 340 ºC for HDO of m-cresol. Conversion (×); methylcylohexanone (♦); methylcyclohexenes (●), methylcyclohexane (■), toluene (▲).

Fig. 10. Conversion and selectivity as function of space time for $NiCo/Al_2O_3$ catalysts at 4 MPa and 340 ºC for HDO of m-cresol. Conversion is shown as bars (left axis), methylcylohexanone (♦), methylcyclohexenes (●), methylcyclohexane (■), toluene (▲).

Scheme 1. Reaction scheme of m-cresol at 340 ºC under 4 MPa over $NiCo/Al_2O_3$.

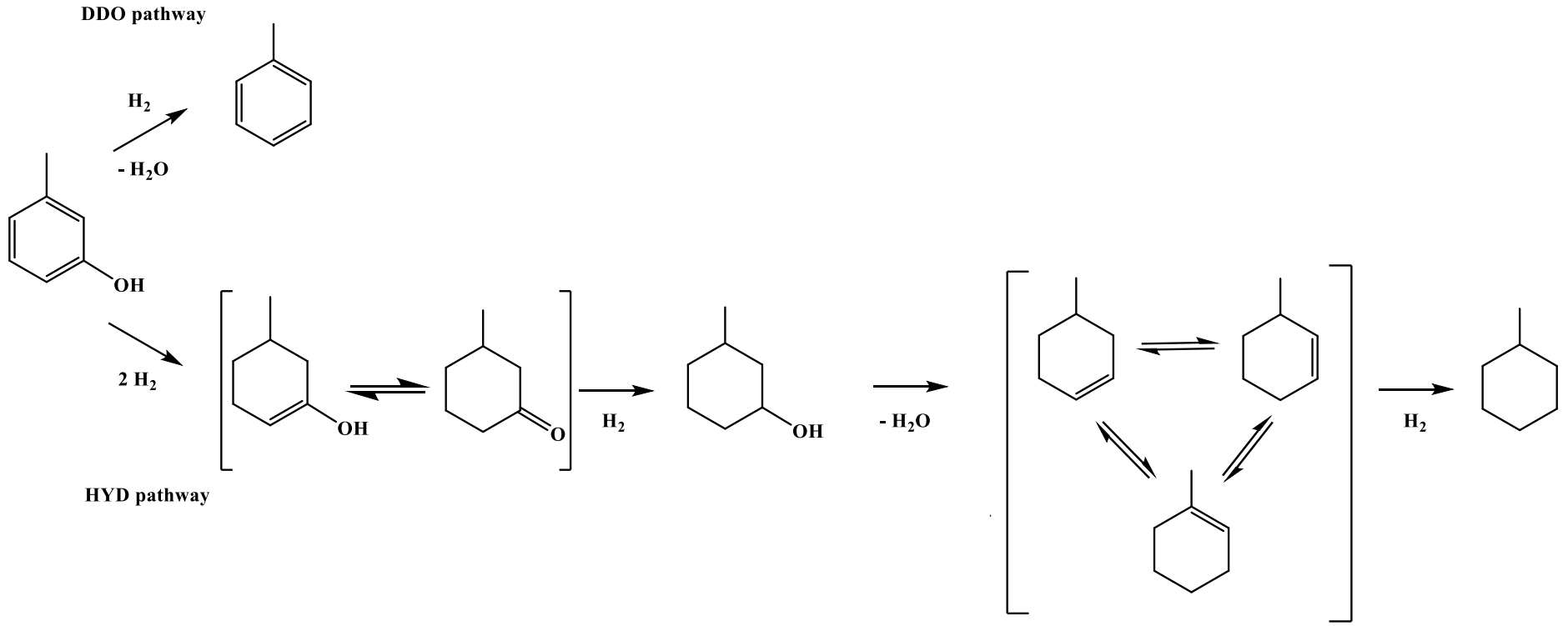

Table 1. Textural properties

Solid	Content (wt.%)		Oxide samples			Reduced samples		
	Ni	Co	S_{BET} ($m^2\ g^{-1}$)	Pore volume ($cm^3\ g^{-1}$)	Average pore diameter (nm)	S_{BET} ($m^2\ g^{-1}$)	Pore volume ($cm^3\ g^{-1}$)	Average pore diameter (nm)
Al_2O_3	-	-	251	0.77	12	-	-	-
Ni/Al_2O_3	9.7	-	197 (225)[a]	0.54 (0.62)[a]	11	193 (220)[a]	0.53 (0.60)[a]	10
$NiCo(3:1)/Al_2O_3$	7.4	2.7	196 (225)[a]	0.52 (0.60)[a]	10	190 (218) [a]	0.51 (0.58)[a]	10
$NiCo(1:1)/Al_2O_3$	5.1	5.3	191 (220)[a]	0.51 (0.59)[a]	10	187 (215)[a]	0.51 (0.59)[a]	10
$NiCo(1:3)/Al_2O_3$	7	2.7	186 (212)[a]	0.49 (0.56)[a]	10	183 (209)[a]	0.49 (0.56)[a]	10
Co/Al_2O_3	-	10.1	194 (223)[a]	0.52 (0.60)[a]	11	192 (220)[a]	0.51 (0.58)[a]	11

a: in brackets are values determined after correction due to the contribution of the weight gain consecutive to the introduction of oxide phases

Table 2. Properties of the catalysts

Catalyst	CO uptake ($\mu mol\ g^{-1}$)	H_2 theoretical uptake[a] ($\mu mol\ g^{-1}$)	H_2-TPR uptake ($\mu mol\ g^{-1}$)	NH_3-TPD uptake ($\mu mol\ g^{-1}$)	a (Å)[b]	D[c] (nm)[c]
Al_2O_3	0	0	0	1.04	-	-
Ni/Al_2O_3	35	1.7	1.8	1.06	3.5347	3.5
$NiCo(3:1)/Al_2O_3$	46	1.8	2.0	nd	3.5374	4.7
$NiCo(1:1)/Al_2O_3$	30	2.0	2.2	1.05	3.5412	6.4
$NiCo(1:3)/Al_2O_3$	22	2.1	2.3	nd	3.5448	8
Co/Al_2O_3	18	2.3	2.4	1.03	3.548	6.5

a: calculated from $NiO + H_2 \rightarrow Ni^0 + H_2O$ and $Co_3O_4 + 4H_2 \rightarrow 3Co^0 + 4H_2O$

b: lattice parameter determined from XRD using Rietveld refinements.

c: particle size determined from XRD using Rietveld refinements

Table 3. Carbon content in the spent catalysts after 25 h on stream at 4 MPa and 340 ºC.

Catalyst	C (wt %)
Ni/Al_2O_3	4.7
$NiCo(3:1)/Al_2O_3$	5.8
$NiCo(1:1)/Al_2O_3$	4.7
$NiCo(1:3)/Al_2O_3$	5.0
Co/Al_2O_3	5.6

Table 4. Product distribution of m-cresol at 340 °C under 4 MPa of total pressure over $NiCo/Al_2O_3$.

Catalyst	τ (g h mol^{-1})	X_{CRE} (%)	k_{TOT}[b] (mmol g^{-1} h^{-1})	TOF (h^{-1})	Selectivity (mol %)				1-MCHe/ MCHes[c]	MCH/ MCHes[d]	HDO (mol %)[e]
					Tol	3-MCHnone	MCHes	MCH			
Ni/Al_2O_3	5.0	19.2	42.6	1217	1.4	15.3	34.1	49.0	0.63	1.4	84
$NiCo(3:1)/Al_2O_3$	5.0	22.3	50.4	1096	1.5	10.1	32.7	55.7	0.63	1.7	90
$NiCo(1:1)/Al_2O_3$	9.0	19.9	27.8	927	1.7	9.2	34.8	54.3	0.64	1.6	91
$NiCo(1:3)/Al_2O_3$	20.0	22.3	13.2	600	2.0	7.9	39.9	50.2	0.63	1.3	92
Co/Al_2O_3	41.0	20.8	5.7	317	6.1	3.9	49.0	41.0	0.64	0.8	96
Ni/Al_2O_3 + Co/Al_2O_3[a]	8.0	20.7	29.0	nd	1.6	12.6	34.5	51.3	0.643	1.5	87

a: Physical mixture of 0.75 Ni/Al_2O_3 and 0.25 Co/Al_2O_3

b: standart deviation of rate constants close to 5%

c 1-MCHe/MCHEs: ratio of 1-methylcyclohexene on all methylcyclohexene isomers

d: MCH/MCHes: ratio of methylcyclohexane on all methylcyclohexene isomers

e: HDO: percentage of deoxygenated products

Fig. 1. N_2 adsorption and desorption isotherms of the bare support and the reduced catalysts at 4 MPa and 340 ºC for 3h. (●) Adsorption (○) Desorption.

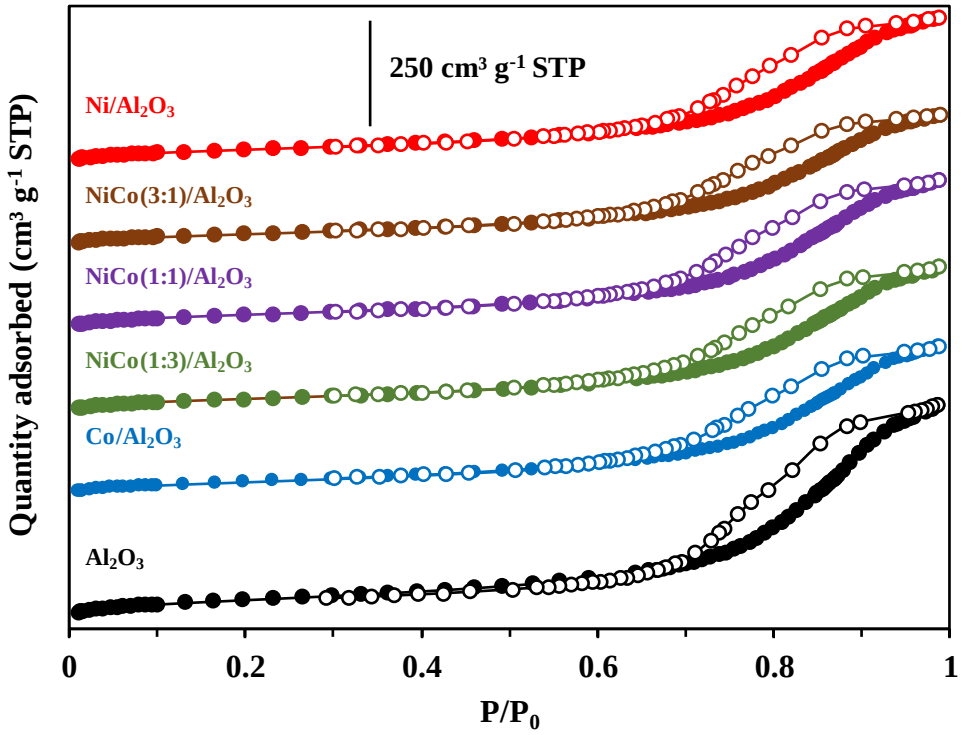

Fig. 2. H_2-TPR profiles of samples with different nickel and cobalt contents. Reduction conditions: 30 ml min^{-1} 10% of H_2 in Ar and heating rate 5 °C min^{-1}.

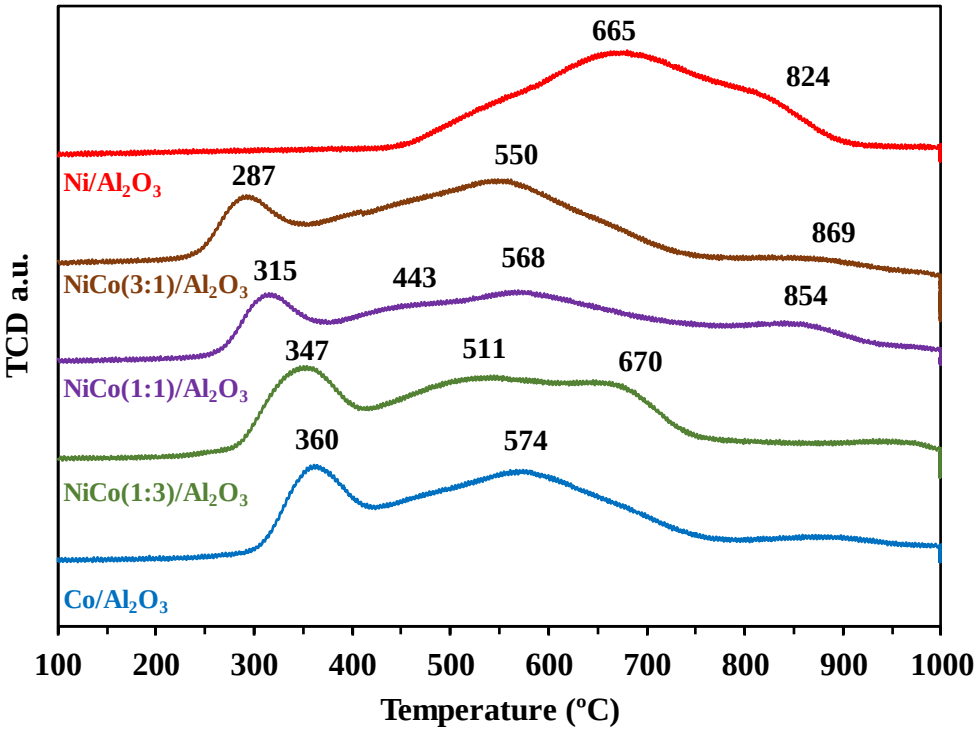

Fig. 3. XRD patterns of reduced samples at 500 ºC under 4 MPa of H_2. Al_2O_3: (◊, JCPDS: 00-050-0741); Ni^0: (▲, JCPDS: 98-016-2279); Co^0: (□: JCPDS: 98-062-2443), Ni-Co solid solution alloy (■).

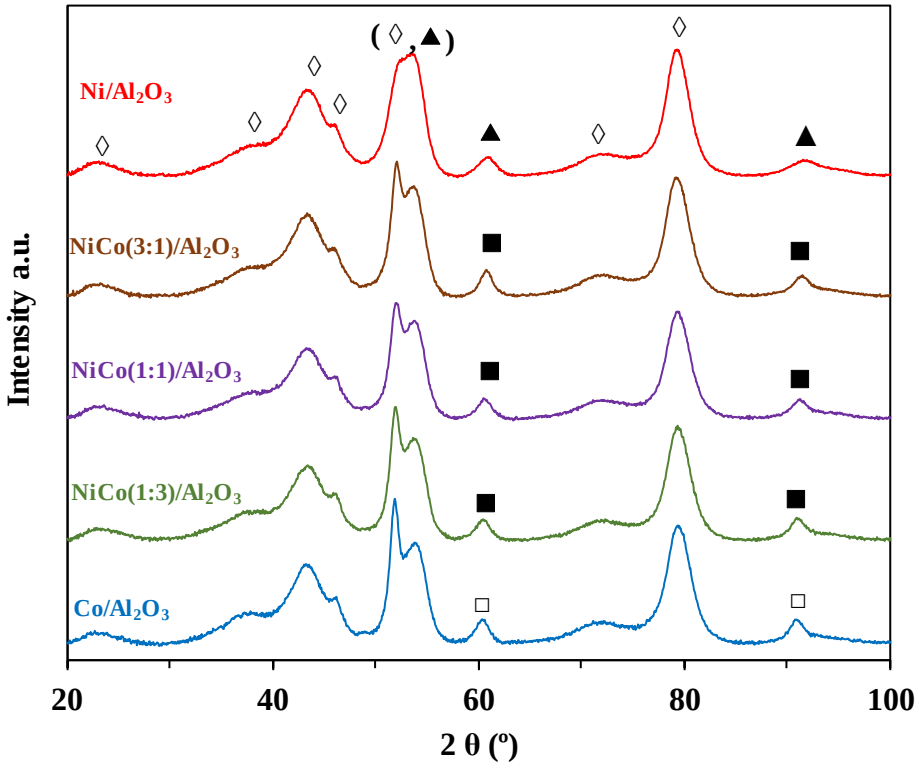

Fig. 4: XRD diagram of Co/Al_2O_3 (a) and $NiCo(3:1)/Al_2O_3$ (b) samples (experimental data (black dots), refined data (red solid line)). Difference between the experimental data and the Rietveld refinement is given at the bottom of the figures.

(a): Co/Al_2O_3

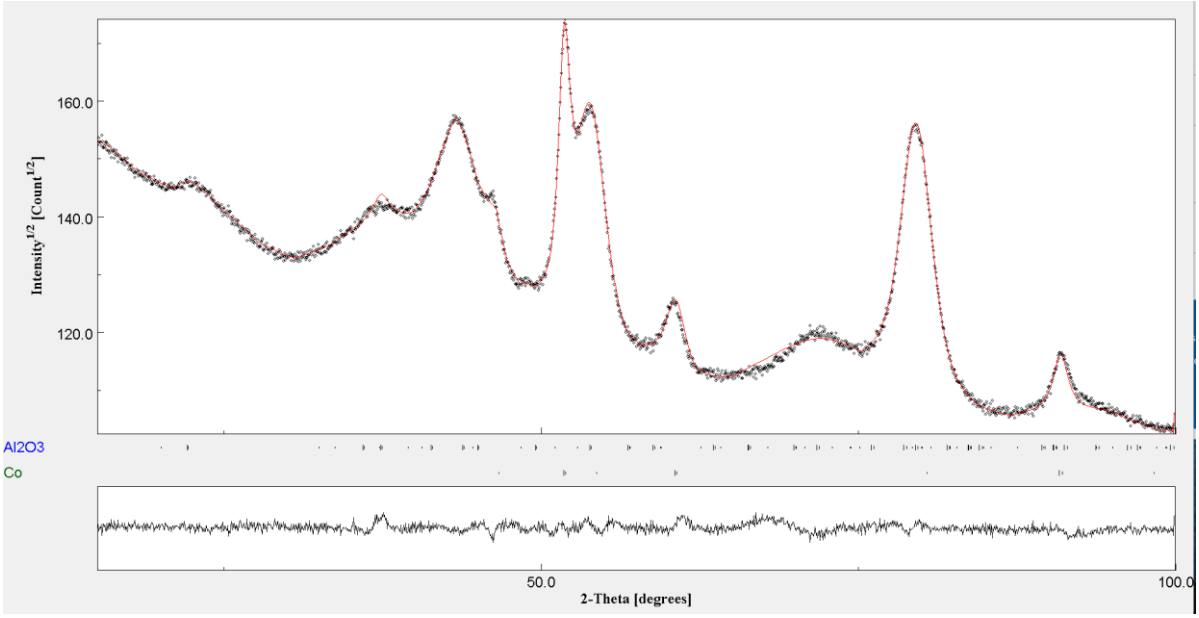

(b): $NiCo(3:1)/Al_2O_3$

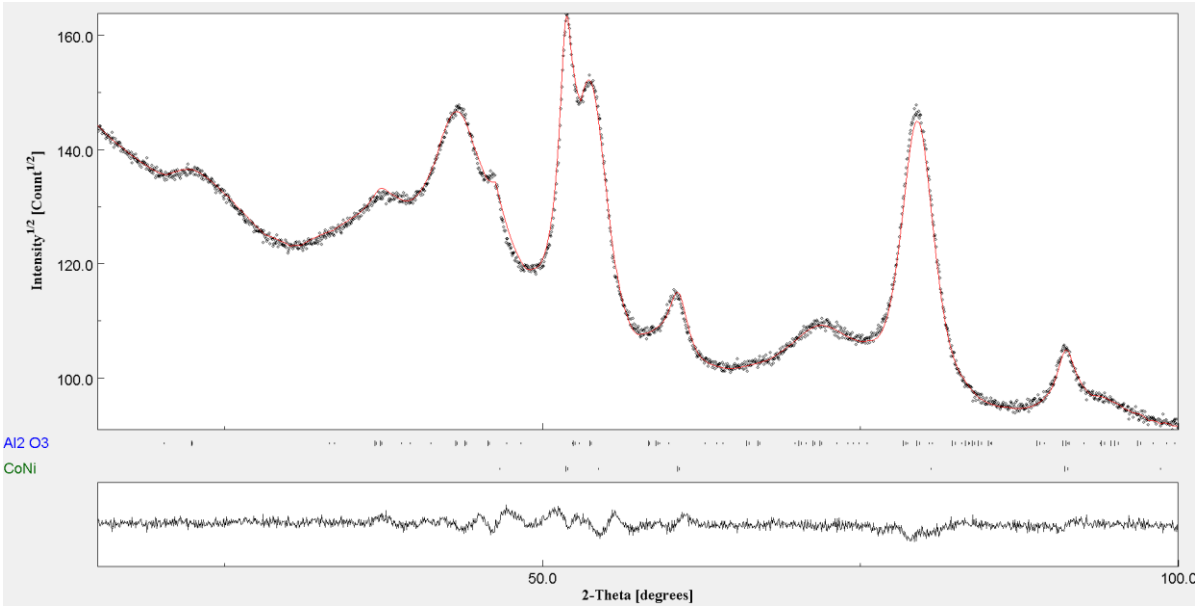

Fig. 5. Influence of the Ni/(Ni + Co) ratio on the lattice parameter (in Å, ■) and the particle size (in nm, ▲) determined from XRD of reduced Ni-Co supported catalysts.

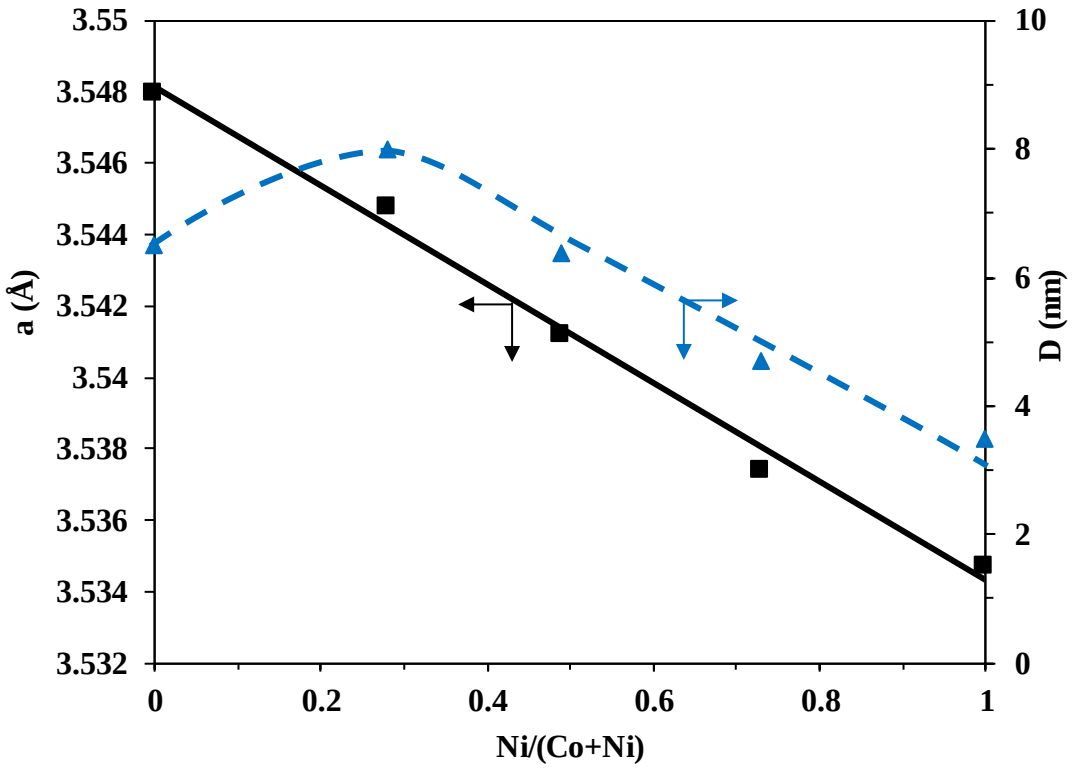

Fig. 6. Conversion as function of time on stream for the HDO of m-cresol during 25 h on stream (τ in g h mol^{-1}).

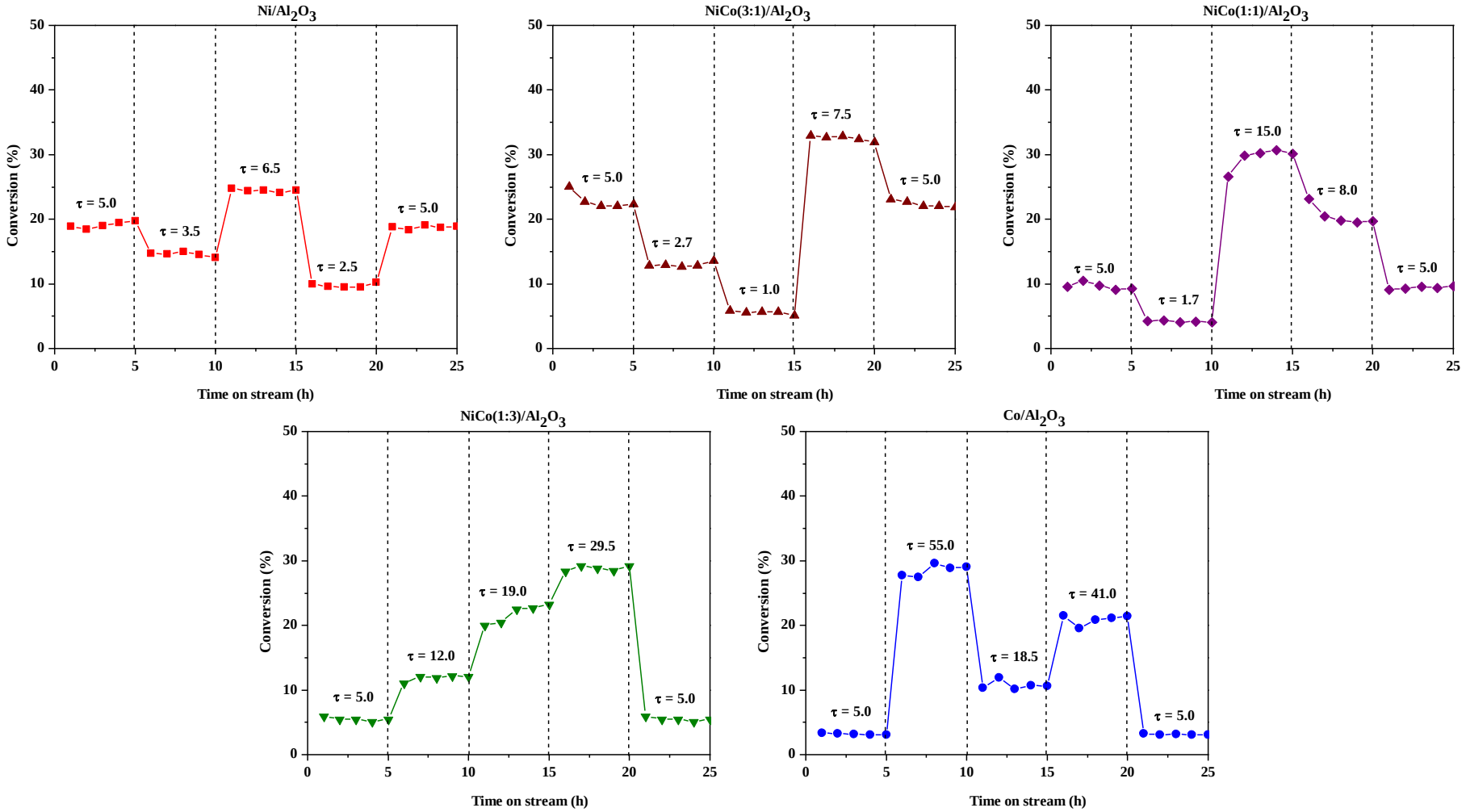

Fig. 7. Plots of -ln (1- X_{CRE}) as function of τ for HDO of m-cresol at 4 MPa and 340 ºC. Ni/Al_2O_3 (■); NiCo(3:1)/Al_2O_3 (▲); NiCo(1:1)/Al_2O_3 (×); NiCo(1:3)/Al_2O_3 (◆); Co/Al_2O_3 (●).

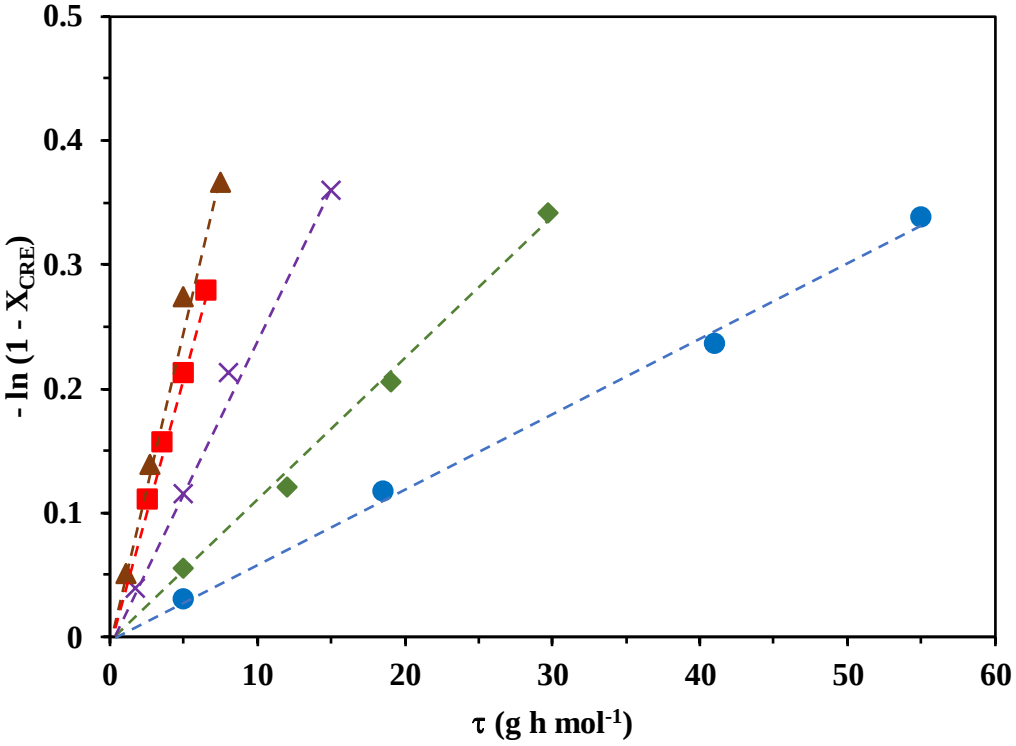

Fig. 8. Influence of the Ni/(Ni+Co) ratio of Al_2O_3 supported catalysts on the k_{TOT} values (■, left axis) obtained for HDO of m-cresol and the CO uptakes (▲, right axis). Mechanical mixture composed by Ni/ Al_2O_3 (75 wt.%) and Co/Al_2O_3 (25 wt.%): k_{TOT} (□) and CO uptake (△).

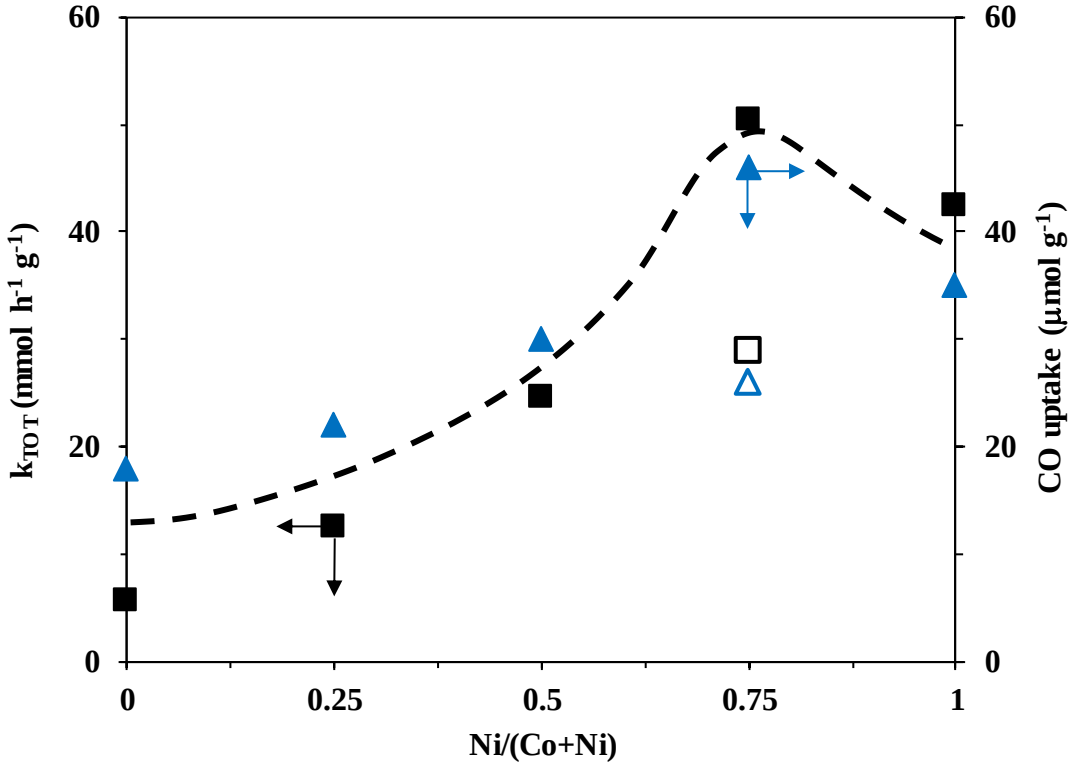

Fig. 9. Conversion and selectivity as function of time on stream for NiCo (3:1)/Al_2O_3 at τ = 5 g h mol^{-1} for HDO of m-cresol. Conversion (×); methylcylohexanone (♦); methylcyclohexenes (●), methylcyclohexane (■), toluene (▲).

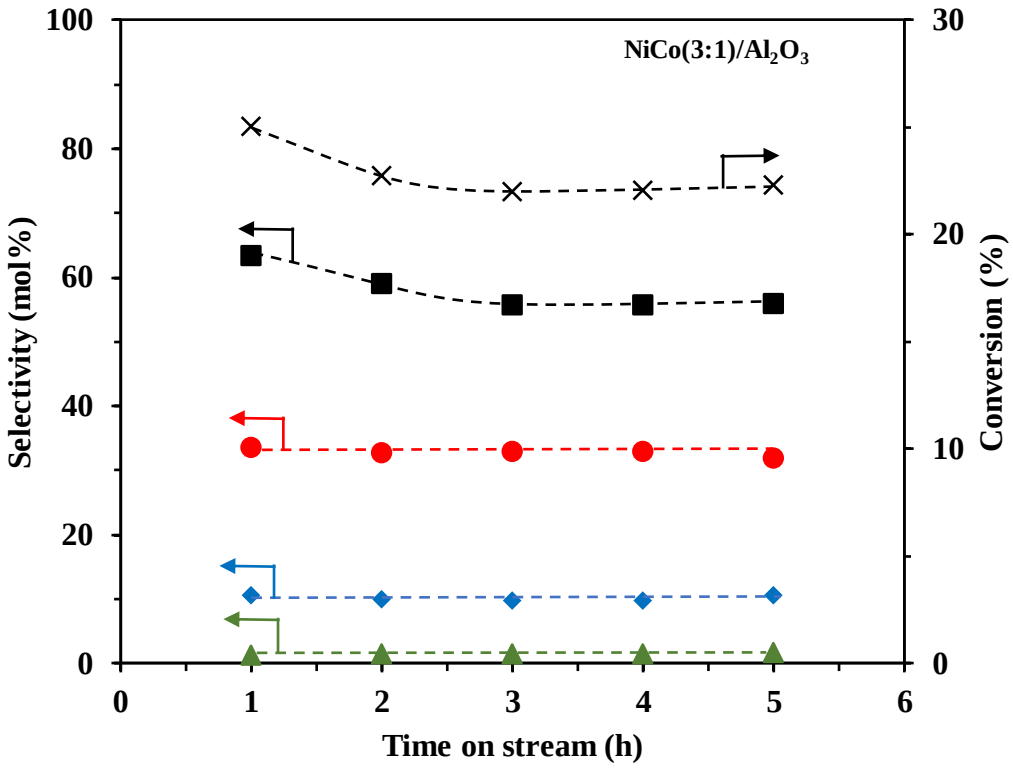

Fig. 10 conversion and selectivity as function of space time for $NiCo/Al_2O_3$ catalysts at 4 MPa and 340 ºC for the transformation of m-cresol. Conversion is shown as bars, methylcylohexanone (♦), methylcyclohexenes (●), methylcyclohexane (■), toluene (▲).